# A Robust Backstepping High-Order Sliding Mode Control Strategy for Grid-Connected DG Units with Harmonic/Interharmonic Current Compensation Capability

Nima Mahdian Dehkordi, Nasser Sadati, *Member, IEEE* and Mohsen Hamzeh, *Member, IEEE*

*Abstract*—This paper presents a new nonlinear current control strategy based on backstepping control and high-order sliding mode differentiator in order to employ distributed generation (DG) unit interfacing converters to actively compensate harmonics/interharmonics of local loads. The converter-based DG unit is connected to a weak grid (with uncertain impedance) and local load (that can be parametrically uncertain and topologically unknown) through an LCL filter. The proposed strategy robustly regulates the inverter output currents and delivers pure sinusoidal, three-phase balanced currents to the grid. The new controller demonstrates the robust performance and robust stability of the DG unit system with respect to the filter parameters uncertainties, grid impedance, grid frequency, and grid voltage as well as the unknown load dynamics that include unbalanced loads and nonlinear loads with harmonic and interharmonic currents. We should remark that the local compensation of the loads with interharmonic current using a DG unit system is first proposed in this paper. When compared with the popular parallel proportional resonant (PR) control technique, the proposed controller offers smoother transient responses and a lower level of current distortion. The performance of the proposed control strategy is verified in MATLAB/SimPowerSystems toolbox.

*Index Terms*—Backstepping control, harmonic compensation, high-order sliding mode differentiator, interharmonic current, nonlinear and unbalanced loads.

## I. INTRODUCTION

The increased application of nonlinear loads such as computers, variable-speed drives, and compact fluorescent lamps, as well as power-electronics-based distributed generation (DG) systems may lead to distribution system harmonic pollutions. To compensate distribution system harmonic issues, a number of active and passive filtering approaches have been proposed [1]. Conversely, installing additional filters is not cost effective. Simultaneously, renewable energy sources (RES) are connected to the grid using current-controlled voltage source converters with output L-type or LCL-type filters [2], [3]. Although grid-connected DG units may introduce harmonics into the power system and distort the power quality of the distribution system, they are also able to improve the distribution system power quality by cancelling the harmonic currents of local loads through modifying control references [4]–[8].

N. Mahdian and N. Sadati are with the Department of Electrical Engineering, Sharif University of Technology, Tehran 11365-9363, Iran (e-mail: mahdian_dehkordi@ee.sharif.edu; sadati@sharif.edu). M. Hamzeh is with the Department of Electrical Engineering, Shahid Beheshti University, Tehran 1983963113, Iran (e-mail: mo_ hamzeh@sbu.ac.ir).

To compensate for the local load harmonic current, many types of harmonic extraction approaches have been suggested [9], including instantaneous power (pq) theory [10], second-order generalized integrator (SOGI) [11], the delayed-signal-cancellation-based detection [12], and Fourier transformation-based detection [13]. To reduce the computational burden of DG unit controllers, the harmonic detectionless method has been proposed [6], [14]. The main grid current commonly needs to be free of harmonic distortion. To improve the power quality of the grid current, the DG unit compensates for the harmonic current drawn by the nonlinear loads through injecting harmonic current. Therefore, the grid current will become free of distortion and the result will be good voltage quality at the point of common coupling (PCC). It becomes more important for a weak grid, where the harmonic current flowing through high grid impedance may cause more voltage distortions at the PCC. As a result, the improvement of the distribution system power quality through the proper control strategy of DG is an issue with high potential for engineering solutions [15].

To attain a high-power quality DG, many strategies for harmonic compensation have been investigated. Harmonic compensation methods can be divided into two categories: selective [6], [8], [16], [17] and non-selective schemes [18]–[22]. Many selective harmonic compensation strategies use a current controller based on proportional-integral (PI) control in the rotating reference frame of each harmonic. Others use parallel proportional resonant (PR) controllers (at the fundamental and harmonic frequencies of interest) either in the stationary or rotating reference frame. These approaches are more flexible than non-selective methods, resulting in good harmonic mitigation. Nevertheless, these methods increase the computational burdens of the controller because they require the implementation of separate controllers for each harmonic component.

As an alternative method, non-selective harmonic compensation strategies such as predictive control [23], repetitive control [20], predictive deadbeat control [21], and sliding mode control [22] have been proposed to improve the performance of the DG systems under undesirable load conditions and to reduce the harmonics in the inverter output currents. However, the repetitive control method has a slow response and cannot guarantee robust stability when faced with parametric uncertainties, unmodeled dynamics, and disturbances. Although

predictive and deadbeat controls ensure a fast dynamic response, they are sensitive to system parameters uncertainties. A number of works that combine sliding mode control with conventional control have been proposed for harmonic compensation [22]. They are shown to be insensitive to parametric uncertainties and external disturbances. Although the sliding mode control method reduces harmonics under undesirable load conditions, the undesired chattering phenomenon is a major drawback of sliding mode control causing low power quality and instability.

The idea of harmonic filtering via point of connection (PoC) using current-controlled grid-connected DG has been presented in [5]. This method works according to the shunt active power filter (APF) capability of DG, where the DG unit improves the distribution system power quality by cancelling the harmonic currents of nonlinear loads. Finally, the DG unit delivers an improved source current and PCC voltage with lower total harmonic distortion (THD). Another method uses the concept of resistive APF (R-APF), where the DG unit acts as a small damping resistor at the selected harmonic frequencies [10]. In [6], the hybrid voltage and current control (HCM) method without using any harmonic detection process has been proposed. Feedback linearization technique is used in [2], but it suffers from the possibility of controlling harmonics. In order to tackle frequency deviations in the microgrid, adaptive HCM in [24] has been proposed. The proposed approach improves DG unit steady-state error as well as accomplishes superior harmonic compensation. In [25], the robust hysteresis controller compensates harmonics in specific frequencies. Resonance mitigation in the grid-connected converters has been investigated in [26].

This paper proposes a new nonlinear control strategy to control the current of a converter-based DG unit connected to a weak grid (with uncertain impedance) and a local load (that can be parametrically uncertain and topologically unknown) through an LCL filter. The proposed controller regulates the grid current in a robust way. In the proposed control strategy, the PCC voltage is considered a measurable disturbance signal. To effectively reject the impact of the disturbance signal on the performance of the system, this paper proposes a new backstepping control with an arbitrary order exact differentiator strategy. According to the separation principle, a controller and a differentiator can be designed separately. A differentiator rejects the impact of a disturbance signal and a backstepping control regulates the DG current. The main salient features of the proposed method can be summarized as follows:

1) The use of a new backstepping control with an arbitrary order exact differentiator technique for control of the DG unit systems has not been proposed or investigated before.

2) To the best of our knowledge, local compensation of the load with interharmonic currents, such as induction furnace, to the grid-connected DG unit has not been investigated before.

3) Unlike existing methods, if the harmonic/interharmonic frequency of the local loads is changed, it is not necessary to change the control structure. This leads to a reduction in the steady-state error of the controller.
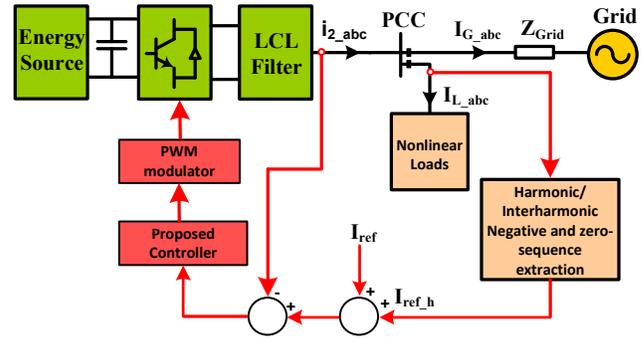


Fig. 1. Compensation scheme for current-controlled DG unit.

4) When compared with the popular parallel PR controllers, the proposed controller offers smoother transient responses with lower levels of current distortion. Moreover, the new controller demonstrates the robust performance and stability of the DG unit system with respect to grid impedance, grid frequency, grid voltage, filter parameters uncertainties, and the unknown load dynamics.

Finally, the simulation results of the proposed controller are compared with those of the conventional parallel PR control method, which confirms the superiority of the proposed nonlinear current controller.

## II. SYSTEM DESCRIPTION AND MATHEMATICAL MODEL

Fig. 1 shows the block diagram of a three-phase, four-wire, grid-connected DG unit, in which a common three-phase voltage-source inverter (VSI) is connected to the grid via an LCL filter. The local loads are connected to the PCC, which are placed at DG unit terminals. As depicted in Fig. 1, the DG output currents are regulated by the proposed controller, while the harmonic extraction block extracts the loads harmonic/interharmonic currents and produce the harmonic/interharmonic currents references to inject a set of pure sinusoidal balanced three-phase grid currents. Fig. 2 shows the circuit diagram of a three-phase four-wire DG unit in grid-connected mode. $L_1$ is the inverter-side inductor along with parasitic resistance; $L_2$ is the grid-side inductor along with parasitic resistance; and $C$ is the filter capacitor.

The state space equations of the DG grid-connected system in the stationary $abc$-frame with the isolation of grid-neutral $N$ can be represented through the following equations:

$$L_1 \dot{i}_{1_{abc}}(t) = u_{abc}(t) - v_{abc}(t) - R_1 i_{1_{abc}}(t)$$
$$C\dot{v}_{abc}(t) = i_{1_{abc}}(t) - i_{2_{abc}}(t)$$
$$L_2 \dot{i}_{2_{abc}}(t) = v_{abc}(t) - R_2 i_{2_{abc}}(t) - V_{PCC_{abc}}(t), \quad (1)$$

where $[i_{1_{abc}}(t)] = [i_{1_a}(t), i_{1_b}(t), i_{1_c}(t)]^T \in R^3$ are the currents of the three-phase inverter referred to point $N$, $[v_{abc}(t)] = [v_a(t), v_b(t), v_c(t)]^T \in R^3$ are the voltages of the three-phase $LCL$ filter capacitor referred to point $N$, $[i_{2_{abc}}(t)] = [i_{2_a}(t), i_{2_b}(t), i_{2_c}(t)]^T \in R^3$ are the currents of the three-phase $LCL$ filter grid-side referred to point $N$, $[V_{PCC_{abc}}(t)] = [V_{PCC_a}(t), V_{PCC_b}(t), V_{PCC_c}(t)]^T \in R^3$ are the voltages of grid referred to neutral point $N$, and
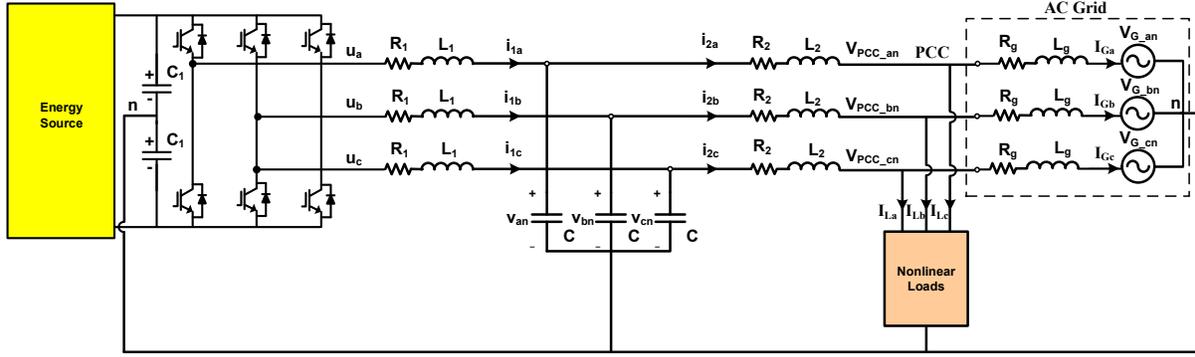
Fig. 2.   Circuit diagram of a three-phase four-wire grid-connected inverter.

$[u_{abc}(t)] = [u_a, u_b, u_c]^T \in R^3$ are the output voltages of the three-phase inverter referred to neutral point $N$ in the stationary $abc$-frame. Because the three-phase grid-connected microgrid contains the neutral point $N$, we analyze separately for each phase. To facilitate the notations, we define new variables for simplicity as $[x_1, x_2, x_3, V_{PCC}, u]^T = [i_{2_a}(t), v_a(t), i_{1_a}(t), V_{PCC_a}(t), u_a(t)]^T$, where $i_{2_a}(t)$, $v_a(t)$, $i_{1_a}(t)$, $V_{PCC_a}(t)$, and $u_a(t) \in R$ denote the single-phase grid-side current, capacitor output voltage, inverter output current, PCC voltage, and control input, respectively. Therefore, we have

$$\dot{x}_1 = \frac{1}{L_2}x_2 - \frac{R_2}{L_2}x_1 - \frac{V_{PCC}}{L_2}$$
$$\dot{x}_2 = \frac{1}{C}x_3 - \frac{1}{C}x_1$$
$$\dot{x}_3 = \frac{1}{L_1}u - \frac{1}{L_1}x_2 - \frac{R_1}{L_1}x_3. \tag{2}$$

Now, if we consider the PCC voltage $V_{PCC}$ a measurable disturbance signal, the state space equations of (2) can be represented strongly as

$$\dot{x}_1 = f_1(x_1) + B_1 x_2 + \zeta_1(t)$$
$$\dot{x}_2 = f_2(x_1, x_2) + B_2 x_3$$
$$\dot{x}_3 = f_3(x_1, x_2, x_3) + B_3 u, \tag{3}$$

where $f_1(x_1)$, $B_1$, $\zeta_1(t)$, $f_2(x_1, x_2)$, $B_2$, $f_3(x_1, x_2, x_3)$, and $B_3 \in R$ are smooth functions as follows:

$$f_1(x_1) = -\frac{R_2}{L_2}x_1, \quad B_1 = \frac{1}{L_2}, \quad \zeta_1 = -\frac{V_{PCC}}{L_2}$$
$$f_2(x_1, x_2) = -\frac{1}{C}x_1, \quad B_2 = \frac{1}{C}$$
$$f_3(x_1, x_2, x_3) = -\frac{1}{L_1}x_2 - \frac{R_1}{L_1}x_3, \quad B_3 = \frac{1}{L_1}. \tag{4}$$

Because $C$, $L_1$, $L_2$, $R_1$, and $R_2$ are considered to be known, then $f_1(x_1)$, $B_1$, $\zeta_1(t)$, $f_2(x_1, x_2)$, $B_2$, $f_3(x_1, x_2, x_3)$, and $B_3 \in R$ are known.

*Assumption 2.1:* The measurable disturbance signal $\zeta_1(t)$ is assumed to be time-varying and known.

## III.  Control Objectives

Given the PCC voltage $V_{PCC}$, the control purpose is to adjust the current waveform of grid side $x_1$ to the desired value $y_c$. Therefore, the state-space equations as well as the output equation are represented as follows:

$$\dot{x}_1 = f_1(x_1) + B_1 x_2 + \zeta_1(t)$$
$$\dot{x}_2 = f_2(x_1, x_2) + B_2 x_3$$
$$\dot{x}_3 = f_3(x_1, x_2, x_3) + B_3 u$$
$$y = x_1, \tag{5}$$

where $f_1(x_1)$, $B_1$, $\zeta_1(t)$, $f_2(x_1, x_2)$, $B_2$, $f_3(x_1, x_2, x_3)$, and $B_3 \in R$ are defined in (4). Moreover, $x_1$, $x_2$, and $x_3$ are considered measurable signals. The control targets are represented as follows:

1) Adjust the current waveform of grid side $x_1$ at the desired value $y_c$, so that the output $y = x_1$ tracks the bounded smooth desired reference $y_c$ with bounded derivatives in the presence of the disturbance $\zeta_1(t) = -\frac{V_{PCC}}{L_2}$ with bounded derivatives, i.e., $|\frac{d^2\zeta_1(t)}{dt^2}| \leq \Gamma$, where $\Gamma$ is a known positive constant. Because the disturbance term $\zeta_1(t)$ acts on a different channel from the control input, the term $\zeta_1(t)$ is called a mismatched disturbance. The mismatched disturbances have been a challenging control problem in microgrid systems. To deal with systems with mismatched disturbances, a new control scheme has been presented.

2) Maintain the quality of the current waveform of the injected current to the grid $I_G$ despite the nonlinear and unbalanced loads, the grid voltage distortion, the grid voltage unbalance, and the other system nonlinearity effects such as the nonlinearity of the inductors.

3) Maintain robust performance in the presence of external disturbances and system uncertainties, including uncertainties in the value of the inverter side filter, grid impedance, and the grid voltage and frequency.

4) Provide harmonic compensation as well as negative and zero sequence compensation for the current waveform of the injected current to the grid $I_G$.

To establish the above goals, the new control scheme has been presented.

## IV.  Proposed Control System

### A.  Backstepping Control

PI controllers and parallel PR controllers are usually applied to the converter-based DG unit. Recently, however, the

backstepping method has been applied to microgrid systems [27]–[30], which allows the designer to incorporate most system nonlinearities and uncertainties into the design of the controller. The backstepping method provides a recursive method for stabilizing the origin of a system or tracking the desired trajectory in strict-feedback form [31]. Moreover, the adaptive backstepping method is applied to the hybrid microgrid to guarantee large signal stability and robustness against unmodeled dynamics, thereby enhancing the system performance [30], [32], [33]. Recently, an adaptive backstepping-sliding mode control method has been employed to design the nonlinear controller of a microgrid system [34]. The proposed method can not only overcome the system nonlinearities and uncertainties, it can also improve the performance of robustness. The existence of parametric uncertainties and disturbances complicates the synthesis of backstepping controllers. In particular, mismatched disturbances limit the application of backstepping techniques [35]. In this section, inspired by the backstepping method, the design procedure for system (5) under the Assumption 2.1 is followed. The main goal of the design is to minimize the error between the desired reference signal $y_c$ and its actual value $y = x_1$ so that the system remains globally stable. The output tracking error can be defined as

$$e_1 = y - y_c. \tag{6}$$

By differentiating (6) and substituting from (5), (7) is obtained.

$$\begin{aligned} \dot{e}_1 &= \dot{y} - \dot{y}_c \\ &= f_1(x_1) + B_1 x_2 + \zeta_1 - \dot{y}_c. \end{aligned} \tag{7}$$

In (7), $x_2$ is treated as the virtual input. Therefore, we define $\phi_1$ as the ideal value of $x_2$ that can control $x_1$ appropriately. To stabilize (7), considering the positive definite Lyapunov function as

$$V_1 = \frac{1}{2} e_1^2. \tag{8}$$

The derivative of (8) along its trajectory is

$$\dot{V}_1 = e_1 \dot{e}_1 = e_1 (f_1(x_1) + B_1 x_2 + \zeta_1 - \dot{y}_c). \tag{9}$$

From the Lyapunov function method of finding the stability, if we make $\dot{V}_1$ negative definite, the system (9) becomes asymptotically stable. Therefore, choose ideal $x_2$ as

$$\phi_1 = \frac{1}{B_1}(-f_1(x_1) - \zeta_1 + \dot{y}_c + H_1 e_1). \tag{10}$$

As a result,

$$\dot{V}_1 = H_1 e_1^2 \le 0, \tag{11}$$

where $H_1$ is selected negative. Because $V_1$ is positive definite and its time derivative $\dot{V}_1$ is negative definite, by virtue of (8) and (11) from the Lyapunov function method of finding the stability, the error $e_1$ converges exponentially to zero−−that is, y converges exponentially to $y_c$. In the next step, according to the backstepping method, consider the error between the ideal and actual $x_2$ as

$$e_2 = x_2 - \phi_1.$$

Next, choose the Lyapunov function as

$$V = \frac{1}{2} e_1^2 + \frac{1}{2} e_2^2, \tag{12}$$

whose derivative is

$$\begin{aligned} \dot{V} &= e_1 \dot{e}_1 + e_2 \dot{e}_2 \\ &= e_1(f_1(x_1) + B_1 x_2 + \zeta_1 - \dot{y}_c) + e_2(\dot{x}_2 - \dot{\phi}_1) \\ &= e_1(f_1(x_1) + B_1(e_2 + \phi_1) + \zeta_1 - \dot{y}_c) + e_2(f_2(x_1, x_2) \\ &\quad + B_2 x_3 - \dot{\phi}_1). \end{aligned} \tag{13}$$

Substituting for $\phi_1$ from (10) yields

$$\dot{V} = H_1 e_1^2 + e_1 B_1 e_2 + e_2(f_2 + B_2 x_3 - \dot{\phi}_1). \tag{14}$$

Similar to the previous step in the backstepping method, we consider equation (14) and regard $x_3$ as its input. We define $\phi_2$ as the ideal value of $x_3$ that can control $x_2$ appropriately according to (15).

$$\phi_2 = \frac{1}{B_2}(-f_2(x_1, x_2) + \dot{\phi}_1 + H_2 e_2 - B_1 e_1). \tag{15}$$

Substituting (15) into (14) yields

$$\dot{V}_2 = H_1 e_1^2 + H_2 e_2^2 \le 0, \tag{16}$$

where $H_1$ and $H_2$ have negative values. By virtue of (16) and (12), $e_1$ and $e_2$ converge exponentially to zero−−that is, y and $\phi_1$ converge exponentially to $y_c$ and $x_2$, respectively. Following the backstepping method, consider now that the error between the ideal and actual $x_3$ is defined by

$$e_3 = x_3 - \phi_2.$$

We select the final Lyapunov function as follows:

$$V = \frac{1}{2} e_1^2 + \frac{1}{2} e_2^2 + \frac{1}{2} e_3^2. \tag{17}$$

Taking the time-derivative of the Lyapunov function (17) and substituting $\phi_2$ from (15) yields

$$\begin{aligned} \dot{V} &= e_1 \dot{e}_1 + e_2 \dot{e}_2 + e_3 \dot{e}_3 \\ &= H_1 e_1^2 + H_2 e_2^2 + e_2 B_2 e_3 + e_3(\dot{x}_3 - \dot{\phi}_2) \\ &= H_1 e_1^2 + H_2 e_2^2 + e_2 B_2 e_3 + e_3(f_3(x_1, x_2, x_3) + B_3 u - \dot{\phi}_2). \end{aligned} \tag{18}$$

Finally, the control law is calculated as

$$u = \frac{1}{B_3}(-f_3(x_1, x_2, x_3) + \dot{\phi}_2 + H_3 e_3 - B_2 e_2). \tag{19}$$

Substituting $u$ from (19) into (18) yields

$$\dot{V} = H_1 e_1^2 + H_2 e_2^2 + H_3 e_3^2 \le 0, \tag{20}$$

where similar to $H_1$ and $H_2$, $H_3$ has a negative value. By virtue of (17) and (20), according to the Lyapunov stability criterion, $e_1$, $e_2$, and $e_3$ exponentially converge to zero−−that is, y, $\phi_1$, and $\phi_2$ converge exponentially to $y_c$, $x_2$, and $x_3$, respectively. These convergences imply that the control input (19) causes the output $y$ exponentially tracks the reference $y_c$ in the presence of disturbance $\zeta_1(t)$; but as seen in (15), (10), and (19), disturbance $\zeta_1(t)$ is used in $\phi_1$, the time-derivative of $\phi_1$ is used in $\phi_2$, and the time-derivative of $\phi_2$ is used in the control signal $u$. The important problem here is the

This article has been accepted for publication in a future issue of this journal, but has not been fully edited. Content may change prior to final publication. Citation information: DOI 10.1109/TSTE.2016.2611383, IEEE Transactions on Sustainable Energy

5

use of the time-derivative of the disturbance signal $\zeta_1(t)$ and the explicit differentiation sensitivity to input noises. For this reason, the controller is not proper and cannot be implemented. Therefore, the backstepping method cannot guarantee robust stability when faced with mismatched disturbances. To solve this problem, a backstepping controller is applied in combination with a high-order sliding mode technique.

### B. Backstepping Control With Arbitrary Order Exact Differentiator

Because the backstepping method cannot guarantee robust stability when faced with mismatched disturbances, we solve this problem using a method derived from [35], applying a backstepping controller in combination with a high-order sliding mode technique. If nothing is known about the structure of the signal except some differential inequalities, high-order sliding modes are used. The arbitrary-order robust exact differentiator [36] is used to compensate for the disturbance to the system (5). In fact, the arbitrary-order robust exact differentiator has been introduced to calculate the time derivatives of the virtual control laws $\phi_1$ and $\phi_2$ in (15) and (19) containing both disturbances and uncertainties. The disturbances have been exactly compensated by the injection of a continuous term generated by the robust exact high-order sliding-modes differentiator.

This differentiator has exact convergence to the true value of the estimated derivatives and provides a degree of softness to the estimated signal by the appropriate selection of the order of the differentiator. Let $\phi$ be a function to differentiate, under the assumption that there exists a constant $L_1$ such that $\mid \phi^{(r)} \mid \leq L_1$, the differentiation of order $r$ can be expressed as follows:

$$
\begin{aligned}
\dot{z}_0 = v_0 &= z_1 - \lambda_r L_1^{1/r} \left| z_0 - \phi \right|^{(r-1)/r} sign(z_0 - \phi) \\
\dot{z}_k = v_k &= z_{k+1} - \lambda_{r-k} L_1^{1/(r-k)} \left| z_k - v_{k-1} \right|^{(r-k-1)/(r-k)} \\
& \quad sign(z_k - v_{k-1}) \qquad k = 1, ..., r-2 \\
\dot{z}_{r-1} &= -\lambda_1 L_1 sign(z_{r-1} - v_{r-2}).
\end{aligned}
\tag{21}
$$

After a finite-time transient process, we have the following inequality:

$$
\left| z_i - \phi^i \right| = 0, \quad i = 0, ..., r.
\tag{22}
$$

This inequality implies that after a finite-time, we have $z_i \longrightarrow \phi^i$. This controller provides the following properties:

- exact compensation of mismatched disturbances in finite-time;
- exponential exact tracking of a smooth reference signal in the presence of mismatched disturbances;
- high-order sliding modes-based control provides a differentiable control signal that does not contain high-frequency terms and is applied directly to the plant.

*Remark 4.1:* The separation principle is attained for the proposed differentiator. According to the separation principle [36], a controller and a differentiator can be designed separately; so that the combined differentiator-controller output feedback is designed to preserve the specifications of the controller.

### C. Control Law

The derivatives of the virtual control laws $\phi_1$ and $\phi_2$ are obtained by application of the high-order sliding mode differentiator (21) to (15) and (19), with the assumption of $r_1 = 2$ and $r_2 = 3$. Therefore, the derivative of the virtual control law $\phi_1$ is obtained by

$$
\begin{aligned}
\dot{z}_0 = v_0 &= -\lambda_3 L_1^{1/3} \left| z_0 - \phi_1 \right|^{2/3} sign(z_0 - \phi_1) + z_1 \\
\dot{z}_1 = v_1 &= -\lambda_2 L_1^{.5} \left| z_1 - v_0 \right|^{.5} sign(z_1 - v_0) + z_2 \\
\dot{z}_2 &= -\lambda_1 L_1 sign(z_2 - v_1),
\end{aligned}
\tag{23}
$$

and the derivative of the virtual control law $\phi_2$ is obtained by

$$
\begin{aligned}
\dot{z}_{01} = v_{01} &= -\lambda_2 L_2^{.5} \left| z_{01} - \phi_2 \right|^{.5} sign(z_{01} - \phi_2) + z_{11} \\
\dot{z}_{11} &= -\lambda_1 L_2 sign(z_{11} - v_{01}).
\end{aligned}
\tag{24}
$$

The controller parameters are selected in a recursive manner as $\lambda_1 = 1.1$, $\lambda_2 = 1.5$, and $\lambda_3 = 2$ [35], [36]. $L_1$ and $L_2$ are obtained by computer simulation [35], [36]. When we combine the controller (19) and the homogeneous differentiator (21), the control law becomes as follows:

$$
\begin{aligned}
u &= \frac{1}{B_3} (-f_3(x_1, x_2, x_3) + z_{11} + H_3 e_3 - B_2 e_2) \\
\dot{z}_0 = v_0 &= -\lambda_3 L_1^{1/3} \left| z_0 - \phi_1 \right|^{2/3} sign(z_0 - \phi_1) + z_1 \\
\dot{z}_1 = v_1 &= -\lambda_2 L_1^{.5} \left| z_1 - v_0 \right|^{.5} sign(z_1 - v_0) + z_2 \\
\dot{z}_2 &= -\lambda_1 L_1 sign(z_2 - v_1) \\
\dot{z}_{01} = v_{01} &= -\lambda_2 L_2^{.5} \left| z_{01} - \phi_2 \right|^{.5} sign(z_{01} - \phi_2) + z_{11} \\
\dot{z}_{11} &= -\lambda_1 L_2 sign(z_{11} - v_{01}).
\end{aligned}
\tag{25}
$$

The control parameters are the set $H_1 < 0$, $H_2 < 0$, $H_3 < 0$, $L_1 > 0$, and $L_2 > 0$, and the system performance is specified with proper selection of these coefficients. The designer has a high degree of freedom to find the best combination of these system parameters, and the best combination of these parameters is determined by simulations [32], [35], [36]. Therefore, the mismatched disturbances will be exactly compensated by the injection of a continuous term generated by the robust exact high-order sliding-modes differentiator, and the control law (25) will be differentiable and can be directly applied to the system [35], [36].

The complete structure of the proposed controller is shown in Fig. 3. The first part of the controller measures the PCC-voltage and sends it to its main part. The second part of the controller uses a high-order sliding mode differentiator to calculate the time derivatives of the virtual control laws $\phi_1$ and $\phi_2$ in (15) and (19), containing both disturbances and uncertainties, and sends the estimated values to its main part. Finally, the main part of the controller uses backstepping control to provide good performance against unbalanced and nonlinear load conditions as well as weak grid condition.

### V. SIMULATION RESULTS

To verify the performance of the proposed harmonic control strategy, a 10 kVA grid-connected DG unit shown in Fig. 1 has been simulated under various scenarios in MATLAB/SimPowerSystems software environment. The system shown in Fig. 1 operates in grid-connected mode and initially
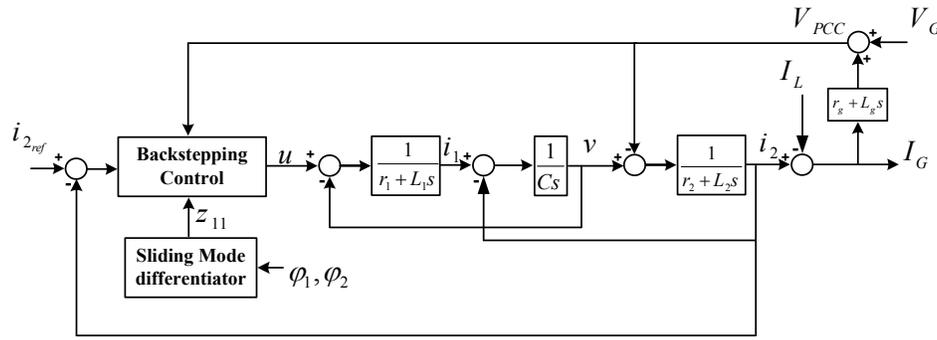
Fig. 3. Structure of the proposed robust controller.

supplies linear unbalanced load of 5 kVA with $PF = 0.9$. The THD of the main grid voltages is about 2%. The system parameters are given in Table I. It is worth mentioning that to verify the robustness of the proposed method with respect to the filter parameters and the grid frequency, the simulations are carried out with a 50% additive uncertainty (i.e., 50% additive deviation from the nominal value) in the filter parameters and a 1% deviation in the grid frequency. The control delay between the sampling instant and duty-cycle update instant also has a great effect on system stability [37]–[39]; therefore, the simulations have been performed under one switching-period control delay (50 $\mu$s). By proper selection of the control parameters, the negative effects of control delay will be compensated for.

TABLE I
PARAMETERS OF THE MICROGRID SYSTEM

| Quantity | Value |
|---|---|
| $R_{f1}$ (series filter resistance) | 0.1 $\Omega$ |
| $R_{f2}$ (series filter resistance) | 0.05 $\Omega$ |
| $L_{f1}$ (series filter inductance) | 2 mH |
| $L_{f2}$ (series filter inductance) | 0.5 mH |
| $C_f$ (shunt capacitance) | 40 $\mu$F |
| $DG$ rated power | 10 kVA |
| $f_{sw}$ (switching frequency) | 10 kHz |
| $V_{ac}$ (phase-neutral voltage of microgrid) | 220 V |
| $f_0$ (system frequency) | 50 Hz |
| $V_{dc}$ (DC bus voltage) | 600 V |

### A. Performance Under Unbalanced Load Condition

Before $t = 0.1$ s, the grid-connected DG unit supplies linear unbalanced load of 5 kVA with $PF = 0.9$. To evaluate the performance of the proposed controller, the reference power of the three-phase inverter has been increased, as shown in Figs. 4(a) and (b). The transient response of the controller is about one cycle (20 ms). Fig. 4(c) shows the good tracking of the reference signals via the controller. As is seen from Fig. 4(e), the error signals of the DG unit are less than 0.1%. Moreover, Fig. 4(d) shows that the harmonic controller injects a set of pure sinusoidal balanced three-phase currents to the main grid. The load currents and control signals of the DG unit are depicted in Figs. 4(a) and (d), respectively. The simulation results of this case study confirm that the proposed control method is strongly robust with respect to the unbalanced loads
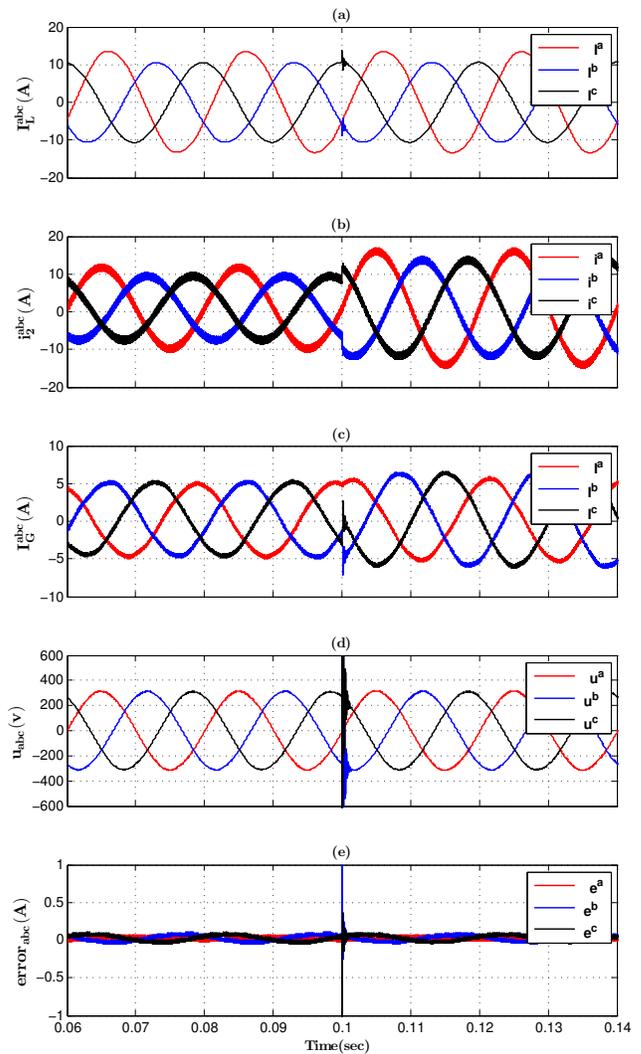


Fig. 4. Performance evaluation of the DG unit with an unbalanced load when the reference power of the three-phase inverter increased at $t = 0.1$ s, resulting in instantaneous (a) load currents, (b) DG currents, (c) grid currents, (d) control signals, and (e) tracking errors.
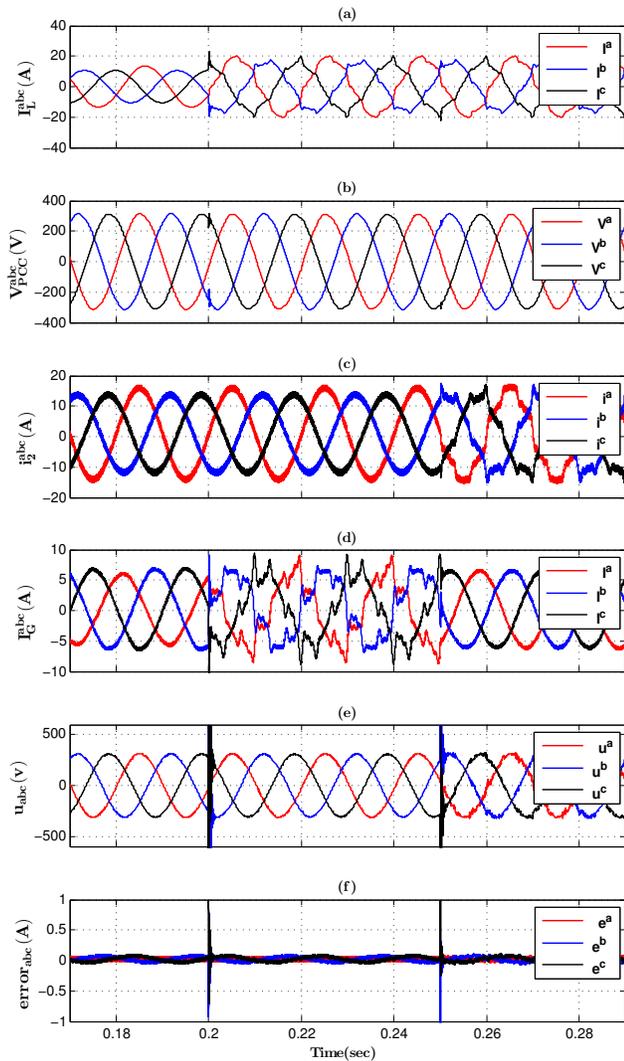
Fig. 5. Performance evaluation of the DG unit with respect to the inclusion of a highly harmonic load, resulting in instantaneous (a) load currents, (b) PCC voltages, (c) DG currents, (d) grid currents, (e) control signals, and (f) tracking errors.

as well as the step changes in the reference power of the three-phase inverter.

### B. Connection of a Three-Phase Harmonic Load

In this section, we investigate the performance of the DG unit with respect to the inclusion of a highly harmonic load, such as a six-pulse rectifier. Subsequent to the previous case study, at $t = 0.2$ s, a six-pulse rectifier with 3 kVA and $PF$ = 0.9 is connected to the PCC.

First, as is seen from Fig. 5(d), subsequent to the inclusion of a six-pulse rectifier load, between $t = 0.2$ s and $t = 0.25$ s, the load harmonic current is not compensated by the DG unit ($I_{ref_h}$=0), and the harmonic load currents flow to the main grid. As a result, the grid currents become highly distorted [where the THD of $I_G^{abc}$ is about 30% as shown in Fig. 11(b)]. As shown in Fig. 5(d), after $t = 0.25$ s, the load harmonic current compensation is applied by setting $I_{ref_h} = I_L$, resulting in the main grid currents $I_G{}^{abc}$ being significantly improved

with a 1.7% THD. Nevertheless, the DG unit currents i$_2$ are polluted with 15% THD, as shown in Fig. 11(c). The control signals and DG currents, shown in Figs. 5(e) and (c), verify that the VSI is injecting harmonic currents to provide the grid currents with a set of pure sinusoidal balanced three-phase currents. The error signals of the DG currents are less than 0.1%, except for a small transient, as shown in Fig. 5(f). The load currents and PCC voltages are depicted in Figs. 5(a) and (b).

To highlight the performance of the proposed controller, we have compared it with the conventional parallel PR controller (more explanation about the PR controller is presented in the Appendix). Fig. 6 shows the performance of the PR controller with a 50% additive uncertainty in the filter parameters. Compared with the proposed method (see Fig. 5(d)), and as it can be seen from Fig. 6(c), the grid currents become distorted and the THD of $I_G^{abc}$ becomes about 8%. Moreover, as shown in Fig. 6(d), the steady-state error of the PR control system is about 0.5 A (10%). As a result, the proposed method has better robustness against uncertainty compared with parallel PR controller.

The simulation results of this case study confirm that the proposed control method is strongly robust with respect to the harmonic load, including a three-phase six-pulse diode-bridge rectifier. Moreover, the proposed controller injects a set of pure sinusoidal balanced three-phase currents with a 1.7% THD to the main grid.

### C. Connection of a Single-Phase Load With Interharmonic Current

In this section, we investigate the performance of the DG unit against the connection a load with an interharmonic current. In this case, a single-phase load that contains the unknown stochastic interharmonic current frequency is employed. At $t = 0.35$ s, a 1.5 kVA single-phase nonlinear load with $PF = 0.9$, including interharmonic current of order 3.5 (175 Hz), is connected to the PCC. The load currents are depicted in Fig. 7(a). The instantaneous DG currents depicted in Fig. 7(b) indicate that the DG unit absorbs the harmonic and interharmonic currents from nonlinear loads and the controller injects a set of pure sinusoidal balanced three-phase currents with a 1.7% THD to the main grid [Fig. 7(c)]. The control signals, depicted in Fig. 7(d), verify that the VSI is injecting interharmonic, negative, and zero-sequence currents in order to provide the DG currents with a set of pure sinusoidal balanced three-phase currents. As seen in Fig. 7(e), the error signals of the DG currents are less than 0.3%.

To highlight the performance of the proposed controller, we have compared it with the parallel PR controller. Fig. 8 shows the performance of the PR controller against the connection of a load with an interharmonic current. Compared with the proposed method, and as can be observed from Fig. 8(c), the grid currents become highly distorted and the THD of $I_G^{abc}$ becomes about 20%. Moreover, the error signals of the current controller become high (see Fig. 8(d)). Consequently, the proposed method shows better robustness against the connection to the PCC of a load with an interharmonic current when
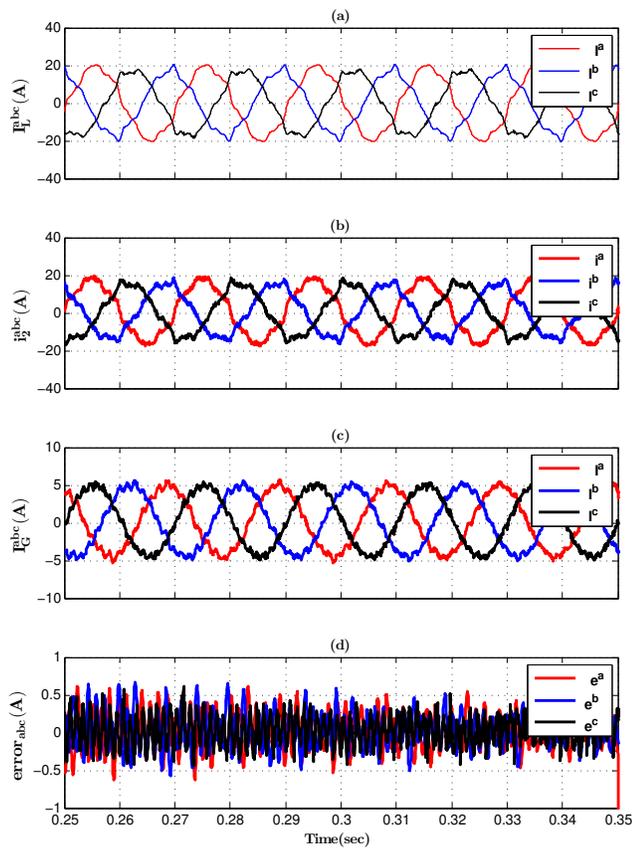
Fig. 6. Performance evaluation of parallel PR controller with respect to the inclusion of a highly harmonic load, resulting in instantaneous (a) load currents, (b) DG currents, (c) grid currents, and (d) tracking errors.

compared with the parallel PR controller. This simulation study verifies the robust performance of the controller with respect to unbalanced load, including an interharmonic current. Moreover, the DG nit currents are sinusoidal with 1.7% THD.

### D. Performance Under Weak Grid Conditions

Weak high-impedance grids may render stability problems. In this section, the effect of increasing the grid impedance is investigated to further evaluate the performance of the controller. At $t = 0.45$ s, the grid impedance is suddenly doubled. Fig. 9(c) shows the current waveforms of the grid, which confirms the controller injects a set of pure sinusoidal balanced three-phase currents with a 1.7% THD to the main grid. As is seen from Fig. 9(e), the error signals of the DG currents are less than 0.1%. Although the DG currents become highly distorted as shown in Fig. 9(b), the grid currents are sinusoidal with 1.7% THD [Fig. 9(c)]. The control signals and DG currents, shown in Figs. 9(d) and (b), verify that the VSI is injecting harmonic currents in order to provide the grid currents with a set of pure sinusoidal balanced three-phase currents. The load currents are depicted in Fig. 9(a). The controller shows an excellent, robust performance with respect to the grid impedance variations. Moreover, all of the simulation results show that the controller has a robust
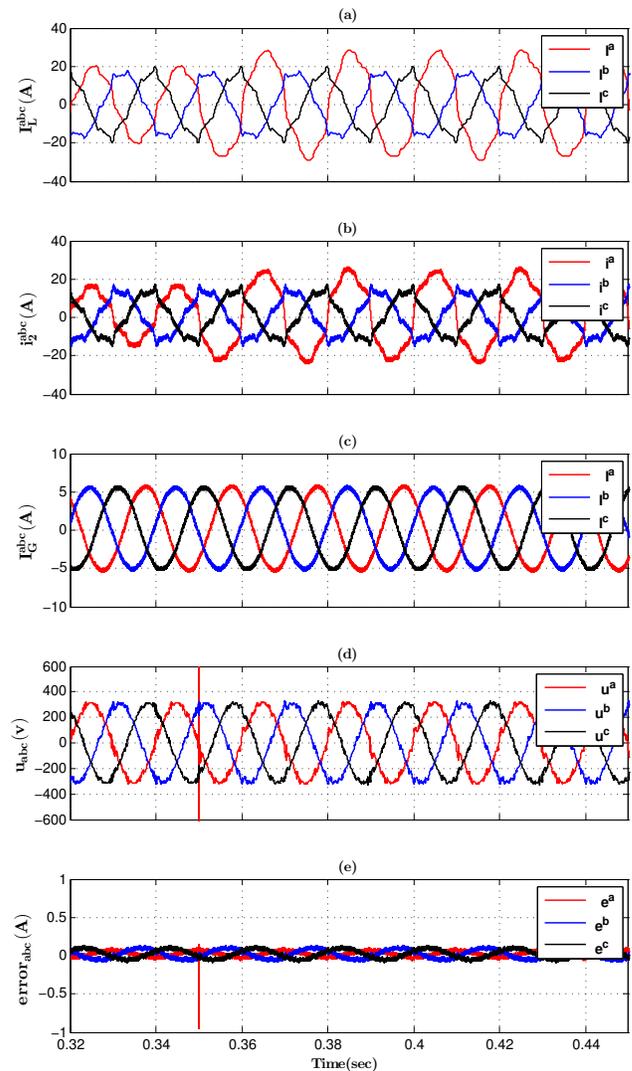


Fig. 7. Performance evaluation of the DG unit when a single-phase nonlinear load (including interharmonic) is connected to the PCC at $t = 0.35$ s, resulting in instantaneous (a) load currents, (b) DG currents, (c) grid currents, (d) control signals, and (e) tracking errors.

performance in the presence of the filter parameters uncertainties. Negative- and zero-sequences and THD criteria are other ways to show the good performance of the controller in the presence of harmonic, interharmonic, and unbalanced loads as well as system uncertainties and disturbances. Uncertainties and disturbances include the value of the filter, grid impedance, grid frequency and unknown faults in the grid. Fig. 10 shows the negative- and zero-sequence components of the load currents, grid currents, and DG currents. As shown in Fig. 11(b), although the load currents are highly distorted [THD of 15% and negative- and zero-sequence of about 4 A according to Fig. 10(a)], the DG unit absorbs the harmonic and interharmonic currents from nonlinear loads and the controller injects a set of pure sinusoidal balanced three-phase currents with a 1.7% THD [negative- and zero-sequence less than 0.3 A according to Fig. 10(b)].
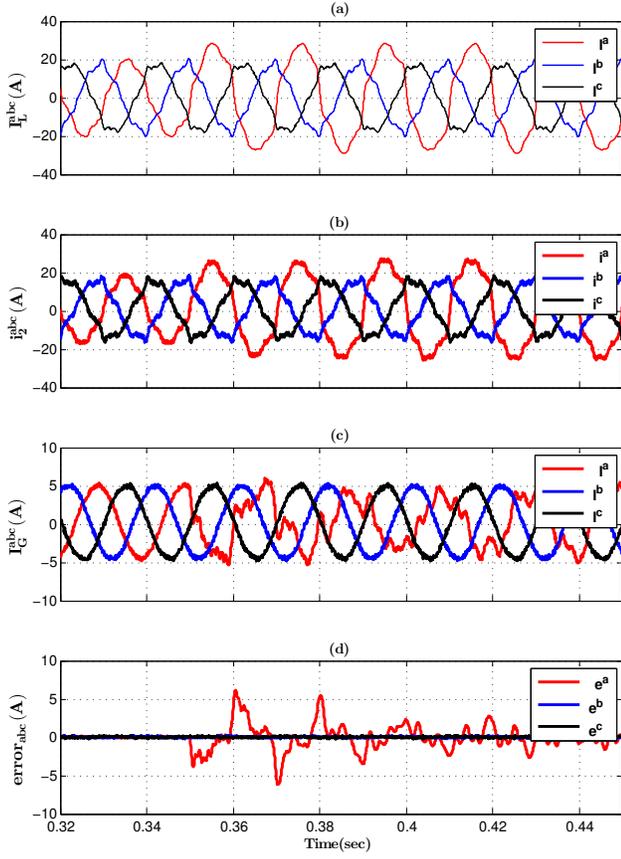
Fig. 8. Performance evaluation of parallel PR controller when a single-phase nonlinear load (including interharmonic) is connected to the PCC at $t = 0.35$ s, resulting in instantaneous (a) load currents, (b) DG currents, (c) grid currents, and (d) tracking errors.

## VI. Conclusion

In this paper, a new harmonic and interharmonic compensation strategy is proposed for DG interfacing converters with LCL filters. The proposed method combines a backstepping control system based on a high-order sliding mode differentiator. The DG unit is connected to a weak grid (with uncertain impedance) and a local load (which can be parametrically uncertain and topologically unknown) through an LCL filter. The PCC voltage is considered a measurable disturbance signal. The aim of the controller is to regulate the grid current, irrespective of the load dynamics, grid impedance, grid frequency, and the grid voltage. To achieve the desirable performance and to reject any disturbance signal, a new backstepping control based on a high-order sliding mode differentiator is proposed. It is worth mentioning that the use of a new backstepping control with an arbitrary order exact differentiator technique for the control of DG grid-connected systems has not been proposed or investigated before. The simulation results confirm that the proposed strategy does the following:

- It maintains the quality of current waveform despite the grid voltage distortion, grid voltage unbalance, and unknown dynamics, including linear, nonlinear, and highly unbalanced loads (such as constant power load) as well
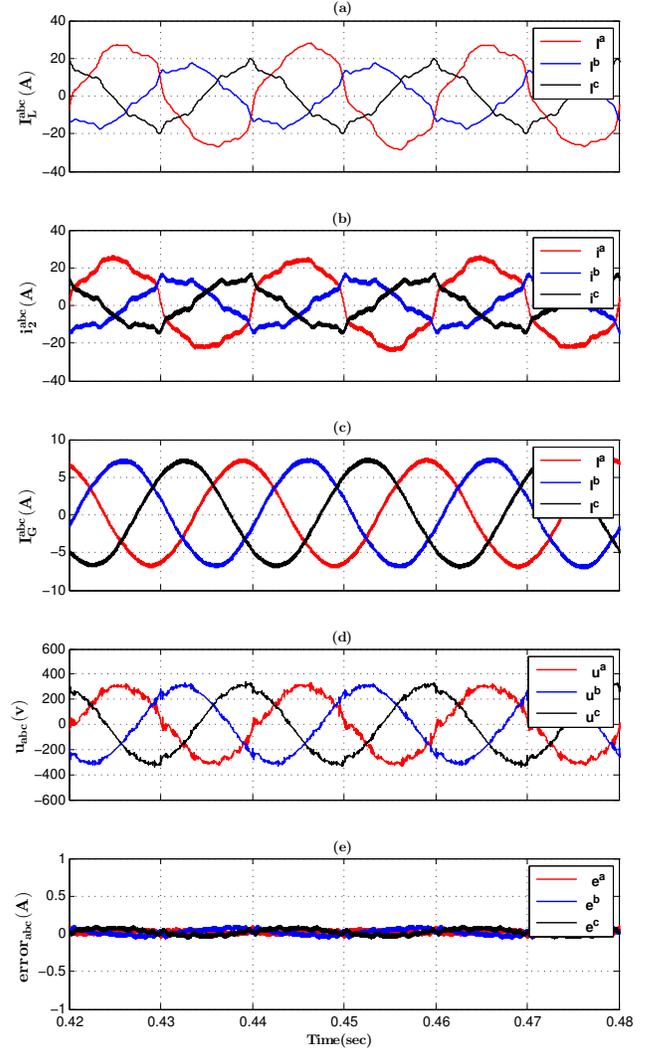


Fig. 9. Performance evaluation of the DG unit when the grid impedance is suddenly doubled at $t = 0.45$ s, resulting in instantaneous (a) load currents, (b) DG currents, (c) grid currents, (d) control signals, and (e) tracking errors.

as loads with an interharmonic current, such as an induction furnace connected to the PCC. To the best of our knowledge, connection of a load with an interharmonic current such as an induction furnace to the DG unit has not been investigated before.

- It accurately compensates for the harmonic currents of nonlinear loads.
- It effectively compensates for the negative- and zero-sequence currents of unbalanced loads.
- It maintains robust performance in the presence of the filter parameters and the grid impedance uncertainties.

## Appendix

The complete structure of the parallel PR controller is expressed as follows:

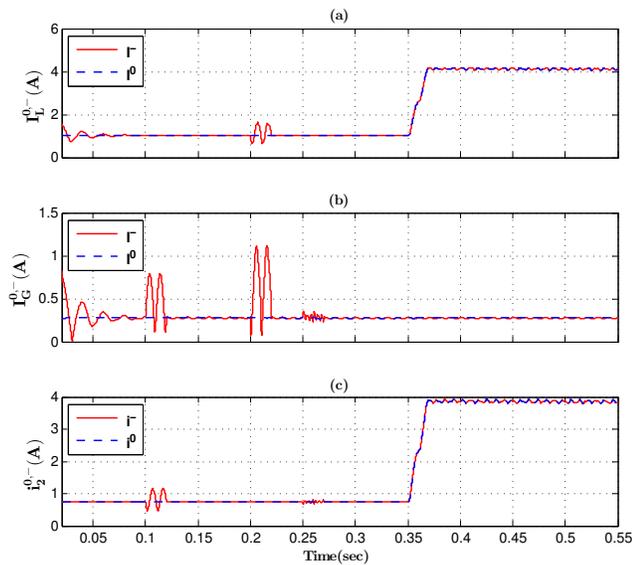$$K(s) = k_g[G_1(s) + G_5(s) + G_7(s) + G_{11}(s) + G_{13}(s)], \tag{26}$$

This article has been accepted for publication in a future issue of this journal, but has not been fully edited. Content may change prior to final publication. Citation information: DOI 10.1109/TSTE.2016.2611383, IEEE Transactions on Sustainable Energy

10

Fig. 10. Negative- and zero-sequences of (a) load currents, (b) grid currents, and (c) DG currents.



Fig. 11. Instantaneous THD of (a) load currents, (b) grid currents, (c) DG currents, and (d) PCC voltages.

where $G_1(s)$, $G_5(s)$, $G_7(s)$, $G_{11}(s)$, and $G_{13}(s)$ are formulated as follows:

$$G_1(s) = k_P + \frac{2k_1\omega_c s}{s^2 + 2\omega_c s + \omega_0^2}, G_5(s) = \frac{10k_5\omega_c s}{s^2 + 10\omega_c s + (5\omega_0)^2}$$

$$G_7(s) = \frac{14k_7\omega_c s}{s^2 + 14\omega_c s + (7\omega_0)^2}$$

$$G_{11}(s) = \frac{22k_{11}\omega_c s}{s^2 + 22\omega_c s + (11\omega_0)^2}$$

$$G_{13}(s) = \frac{26k_{13}\omega_c s}{s^2 + 26\omega_c s + (13\omega_0)^2}. \tag{27}$$

In these equations, the $k_i$ ($i$ = 1, 5, 7, 11, 13) coefficients, $k_p$, and $\omega_c$ are the parameters of the PR controllers that must be determined. To obtain these coefficients, the following criteria must be satisfied:

- rapid reference tracking without steady-state error;
- a gain margin more than 3dB;
- a phase margin more than 30 deg;
- band-width less than 10% of the switching frequency;
- quick disturbance rejection.

Moreover, the parameters of the designed parallel PR controller are shown in Table II.

TABLE II
PARALLEL PR CONTROLLER PARAMETERS.

| $k_p$ | 1 | $k_g$ | 1 |
|---|---|---|---|
| $k_1$ | 5000 | $k_5$ | 4000 |
| $k_7$ | 3000 | $\omega_c$ | .01 |
| $k_{11}$ | 2000 | $k_{13}$ | 2000 |

## REFERENCES

[1] L. Asiminoaei, F. Blaabjerg, S. Hansen, and P. Thogersen, "Adaptive compensation of reactive power with shunt active power filters," *IEEE Trans. Ind. Appl.*, vol. 44, no. 3, pp. 867–877, May 2008.

[2] S. Khajehoddin, M. Karimi-Ghartemani, P. Jain, and A. Bakhshai, "A control design approach for three-phase grid-connected renewable energy resources," *IEEE Trans. Sustain. Energy*, vol. 2, no. 4, pp. 423–432, Oct. 2011.

[3] X. Wu, X. Li, X. Yuan, and Y. Geng, "Grid harmonics suppression scheme for LCL-type grid-connected inverters based on output admittance revision," *IEEE Trans. Sustain. Energy*, vol. 6, no. 2, pp. 411–421, Apr. 2015.

[4] N. Pogaku and T. Green, "Harmonic mitigation throughout a distribution system: A distributed-generator-based solution," *IEEE Proc. Gener. Transm. Distrib.*, vol. 153, no. 3, pp. 350–358, May 2006.

[5] M. Cirrincione, M. Pucci, and G. Vitale, "A single-phase DG generation unit with shunt active power filter capability by adaptive neural filtering," *IEEE Trans. Ind. Electron.*, vol. 55, no. 5, pp. 2093–2110, May 2008.

[6] J. He, Y. W. Li, F. Blaabjerg, and X. Wang, "Active harmonic filtering using current-controlled, grid-connected DG units with closed-loop power control," *IEEE Trans. Power Electron.*, vol. 29, no. 2, pp. 642–653, Feb. 2014.

[7] R. Bojoi, L. Limongi, D. Roiu, and A. Tenconi, "Enhanced power quality control strategy for single-phase inverters in distributed generation systems," *IEEE Trans. Power Electron.*, vol. 26, no. 3, pp. 798–806, Mar. 2011.

[8] J. He, Y. W. Li, and M. Munir, "A flexible harmonic control approach through voltage-controlled DG-grid interfacing converters," *IEEE Trans. Ind. Electron.*, vol. 59, no. 1, pp. 444–455, Jan. 2012.

[9] L. Asiminoaei, F. Blaabjerg, and S. Hansen, "Detection is key-harmonic detection methods for active power filter applications," *IEEE Ind. Appl. Mag.*, vol. 13, no. 4, pp. 22–33, Jul. 2007.

[10] H. Akagi, "Control strategy and site selection of a shunt active filter for damping of harmonic propagation in power distribution systems," *IEEE Trans. Power Del.*, vol. 12, no. 1, pp. 354–363, Jan. 1997.

[11] P. Rodriguez, A. Luna, I. Candela, R. Mujal, R. Teodorescu, and F. Blaabjerg, "Multiresonant frequency-locked loop for grid synchronization of power converters under distorted grid conditions," *IEEE Trans. Ind. Electron.*, vol. 58, no. 1, pp. 127–138, Jan. 2011.

[12] Y. F. Wang and Y. W. Li, "Three-phase cascaded delayed signal cancellation PLL for fast selective harmonic detection," *IEEE Trans. Ind. Electron.*, vol. 60, no. 4, pp. 1452–1463, Apr. 2013.

[13] B. McGrath, D. Holmes, and J. Galloway, "Power converter line synchronization using a discrete fourier transform DFT based on a variable sample rate," *IEEE Trans. Power Electron.*, vol. 20, no. 4, pp. 877–884, Jul. 2005.

[14] J. Miret, M. Castilla, J. Matas, J. Guerrero, and J. Vasquez, "Selective harmonic-compensation control for single-phase active power filter with high harmonic rejection," *IEEE Trans. Ind. Electron.*, vol. 56, no. 8, pp. 3117–3127, Aug. 2009.

[15] M. Manoj Kumar, M. Mishra, and C. Kumar, "A grid-connected dual voltage source inverter with power quality improvement features," *IEEE Trans. Sustain. Energy*, vol. 6, no. 2, pp. 482–490, Apr. 2015.

[16] C. Lascu, L. Asiminoaei, I. Boldea, and F. Blaabjerg, "High performance current controller for selective harmonic compensation in active power filters," *IEEE Trans. Power Electron.*, vol. 22, no. 5, pp. 1826–1835, Sept. 2007.

[17] M. Hamzeh, S. Emamian, H. Karimi, and J. Mahseredjian, "Robust control of an islanded microgrid under unbalanced and nonlinear load conditions," *IEEE J. Emerg. Sel. Topics Power Electron.*, vol. 4, no. 2, pp. 512–520, Jun. 2016.

[18] S. Chen, Y. M. Lai, S. C. Tan, and C. K. Tse, "Analysis and design of repetitive controller for harmonic elimination in PWM voltage source inverter systems," *IET Power Electron.*, vol. 1, no. 4, pp. 497–506, Dec. 2008.

[19] A. Timbus, M. Liserre, R. Teodorescu, P. Rodriguez, and F. Blaabjerg, "Evaluation of current controllers for distributed power generation systems," *IEEE Trans. Power Electron.*, vol. 24, no. 3, pp. 654–664, Mar. 2009.

[20] G. Escobar, P. G. Hernandez-Briones, P. R. Martinez, M. Hernandez-Gomez, and R. E. Torres-Olguin, "A repetitive-based controller for the compensation of Electron., vol. 55, no. 8, pp. 3150–3158, Aug. 2008.

[21] J. R. Fischer, S. A. Gonzlez, I. Carugati, M. A. Herrn, M. G. Judewicz, and D. O. Carrica, "Robust predictive control of grid-tied converters based on direct power control," *IEEE Trans. Power Electron.*, vol. 29, no. 10, pp. 5634–5643, Oct. 2014.

[22] X. Hao, X. Yang, T. Liu, L. Huang, and W. Chen, "A sliding-mode controller with multiresonant sliding surface for single-phase grid-connected VSI with an LCL filter," *IEEE Trans. Power Electron.*, vol. 28, no. 5, pp. 2259–2268, May 2013.

[23] P. Acua, L. Morn, M. Rivera, J. Dixon, and J. Rodriguez, "Improved active power filter performance for renewable power generation systems," *IEEE Trans. Power Electron.*, vol. 29, no. 2, pp. 687–694, Feb. 2014.

[24] J. He, Y. W. Li, and F. Blaabjerg, "Flexible microgrid power quality enhancement using adaptive hybrid voltage and current controller," *IEEE Trans. Ind. Electron.*, vol. 61, no. 6, pp. 2784–2794, Jun. 2014.

[25] P.-C. Tan, P. C. Loh, and D. Holmes, "A robust multilevel hybrid compensation system for 25-kV electrified railway applications," *IEEE Trans. Power Electron.*, vol. 19, no. 4, pp. 1043–1052, Jul. 2004.

[26] Y.-R. Mohamed, "Suppression of low- and high-frequency instabilities and grid-induced disturbances in distributed generation inverters," *IEEE Trans. Power Electron.*, vol. 26, no. 12, pp. 3790–3803, Dec. 2011.

[27] A. Allag, M. Y. Hammoudi, S. M. Mimoune, M. Y. Ayad, M. Becherif, and A. Miraoui, "Tracking control via adaptive backstepping approach for a three phase PWM AC-DC converter," in *Proc. IEEE Int. Symp. Ind. Electron.*, Jun. 2007, pp. 371–376.

[28] B. Parkhideh and S. Bhattacharya, "Vector-controlled voltage-source-converter-based transmission under grid disturbances," *IEEE Trans. Power Electron.*, vol. 28, no. 2, pp. 661–672, Feb. 2013.

[29] A. D. Martin, J. M. Cano, J. F. A. Silva, and J. R. Vzquez, "Backstepping control of smart grid-connected distributed photovoltaic power supplies for telecom equipment," *IEEE Trans. Energy Convers.*, vol. 30, no. 4, pp. 1496–1504, Dec. 2015.

[30] N. Mahdian-Dehkordi, M. Namvar, H. Karimi, P. Piya, and M. Karimi-Ghartemani, "Nonlinear adaptive control of grid-connected three-phase inverters for renewable energy applications," *Int. J. Control*, pp. 1–15, 2015. [Online]. Available: http://dx.doi.org/10.1080/00207179.2015.1086026

[31] H. K. Khalil, *Nonlinear Systems*, 3rd ed. Upper Saddle River, NJ, USA: Prentice-Hall, 2002.

[32] S. M. Ashabani and Y. A. R. I. Mohamed, "A flexible control strategy for grid-connected and islanded microgrids with enhanced stability using nonlinear microgrid stabilizer," *IEEE Trans. Smart Grid*, vol. 3, no. 3, pp. 1291–1301, Sept. 2012.

[33] A. Karimi and A. Feliachi, "Decentralized adaptive backstepping control of electric power systems," *Electric Power Systems Research*, vol. 78, no. 3, pp. 484 – 493, 2008.

[34] Q. Sun, J. Zhou, J. M. Guerrero, and H. Zhang, "Hybrid three-phase/single-phase microgrid architecture with power management capabilities," *IEEE Trans. Power Electron.*, vol. 30, no. 10, pp. 5964–5977, Oct. 2015.

[35] J. Davila, "Exact tracking using backstepping control design and high-order sliding modes," *IEEE Trans. Autom. Control*, vol. 58, no. 8, pp. 2077–2081, Aug. 2013.

[36] A. Levant, "Higher-order sliding modes, differentiation and output-feedback control," *Int. J. Control*, vol. 76, no. 9-10, pp. 924–941, Aug. 2003.

[37] S. Yang, Q. Lei, F. Z. Peng, and Z. Qian, "A robust control scheme for grid-connected voltage-source inverters," *IEEE Trans. Ind. Electron.*, vol. 58, no. 1, pp. 202–212, Jan. 2011.

[38] L. Harnefors, A. G. Yepes, A. Vidal, and J. Doval-Gandoy, "Passivity-based controller design of grid-connected VSCs for prevention of electrical resonance instability," *IEEE Trans. Ind. Electron.*, vol. 62, no. 2, pp. 702–710, Feb. 2015.

[39] J. He, Y. W. Li, F. Blaabjerg, and X. Wang, "Active harmonic filtering using current-controlled, grid-connected DG units with closed-loop power control," *IEEE Trans. Power Electron.*, vol. 29, no. 2, pp. 642–653, Feb. 2014.

**Nima Mahdian Dehkordi** was born in Shahrekord, Iran, on September 20, 1988. He received the B.Sc degree in electrical engineering from the University of Shahrekord, Shahrekord, Iran, in 2010 and the M.Sc. degree in electrical engineering from the Sharif University of Technology, Tehran, Iran, in 2012. He is currently working toward the Ph.D. degree in electrical engineering at Sharif University of Technology, Tehran, Iran. His research interests include control systems, applications of control theories in power electronics, microgrid control, distributed generations, network control, nonlinear control, distributed control, and cooperative control.

**Nasser Sadati** (M'95) is a Full Professor with the Department of Electrical Engineering, Sharif University of Technology, Tehran, Iran, where he is the Director of the Intelligent Systems Laboratory, and the Founder of research on intelligent control of large-scale systems. He has published two control books in Persian and over 280 technical papers in peer-reviewed journals and conference proceedings. His recent book published by Wiley-IEEE Press (2012) is on hybrid control and motion planning of dynamical legged locomotion. His research interests include intelligent control and soft computing, large-scale control systems, robotics, control of biped locomotion, and robust control.

Dr. Sadati is a Technical Committee Member on distributed intelligent systems of the IEEE Systems, Man, and Cybernetics Society.

**Mohsen Hamzeh** (S'09-M'13) received the B.Sc and M.Sc degrees from the University of Tehran, Tehran, Iran, in 2006 and 2008, respectively, and the Ph.D. degree from Sharif University of Technology, Tehran, Iran, in 2012, all in electrical engineering. Since 2010, he has been the Senior Research Engineer with the SGP Company, Tehran, Iran. He joined the Department of Electrical and Computer Engineering, Shahid Beheshti University, Tehran, Iran, in 2013, where he is currently an Assistant Professor. His research interests include renewable energies, microgrid control and applications of power electronics in power distribution systems.